IEEE Access
Multidisciplinary | Rapid Review | Open Access Journal

Received February 21, 2019, accepted May 3, 2019, date of publication May 10, 2019, date of current version May 24, 2019.

Digital Object Identifier 10.1109/ACCESS.2019.2916195

Direct Model Predictive Control of Novel H-Bridge Multilevel Inverter Based Grid-Connected Photovoltaic System

MUHAMMAD BILAL SATTI AND AMMAR HASAN
School of Electrical Engineering and Computer Science (SEECS), National University of Sciences and Technology, Islamabad 44000, Pakistan
Corresponding author: Muhammad Bilal Satti (msatti.msee15seecs@seecs.edu.pk)

ABSTRACT In this paper, a direct model predictive control (DMPC) for the novel H-Bridge multilevel inverter topology-based grid-connected photovoltaic system (GCPS) is presented. The DMPC has several advantages over the conventional control techniques, including optimality, ability to handle multiple control goals, and direct manipulation of semiconductor switches instead of the modulator. The main control goals in the GCPS are to extract the maximum energy from the photovoltaic (PV) system and inject the current into the grid with minimum total harmonic distortion (THD) or close to unity power factor. The DMPC performs well in terms of these control goals. The entire GCPS with the proposed controller is simulated in Simulink MATLAB and the results are compared with the existing GCPSs in the literature. The usage of less number of semiconductor switches while keeping the same number of output voltage levels made the proposed GCPS efficient, less costly, and simpler in design. Moreover, its voltage and current THD are comparable with the systems existing in the literature.

INDEX TERMS Grid-connected photovoltaic systems, model predictive control, multilevel inverter, photovoltaic systems, total harmonic distortion.

I. INTRODUCTION

At present, grid connected photovoltaic systems (GCPS) is one of the key research areas in renewable solar energy. The reasons behind the excessive growth of these systems are the increased demand of energy, environmental benefits of renewable energy, advances in power electronics converters, and the cost reduction of photovoltaic (PV) panels [1], [2]. The key performance criteria of a GCPS are maximum power point (MPP) tracking of PV panels, power conversion efficiency, and total harmonic distortion (THD) of the current injected into the grid. The performance of a GCPS is highly dependent on the choice of the power converter and the control technique.

There are several topologies of power converters that can be employed in a GCPS [3]. One of the most promising class of power converters is the multilevel inverters (MLI). Multilevel inverters have medium to high power handling capability and can include multiple voltage sources or multiple PV panels as an input. A main feature of MLIs is the stair-case like output waveform, which resembles a sinusoid, that has a low THD [4]. In recent years, there has been an increase in the usage of multilevel inverters in applications like smart grids, grid-connected PV systems, induction motor drives and conveyor belts [5], [6]. The three basic topologies of multilevel inverters are diode clamped, flying capacitor and cascaded H-bridge (CHB). CHB is the most common MLI topology due to its modularity, simpler control scheme, and absence of energy storing elements [7], [8]. GCPS based on CHBMLI are the most familiar systems these days due to the diverse advantages of the topology [9], [10]. Another variant of CHB topology, which is presented in [11], is being used in GCPS due to its improved efficiency [12]. The efficiency of the converter is one of its most important performance criteria. Among other things, the efficiency of a converter depends on the number of semiconductor switches. Recently, a new CHB based topology called the novel H-Bridge MLI [4], [13] has been introduced that has an improved efficiency as compared to the basic CHB [6] and the topology in [11]. In this paper, we have considered the novel H-Bridge MLI for the GCPS.

As mentioned earlier, the second key design element that contributes to the performance of GCPS is the employed

The associate editor coordinating the review of this manuscript and approving it for publication was Ramani Kannan.

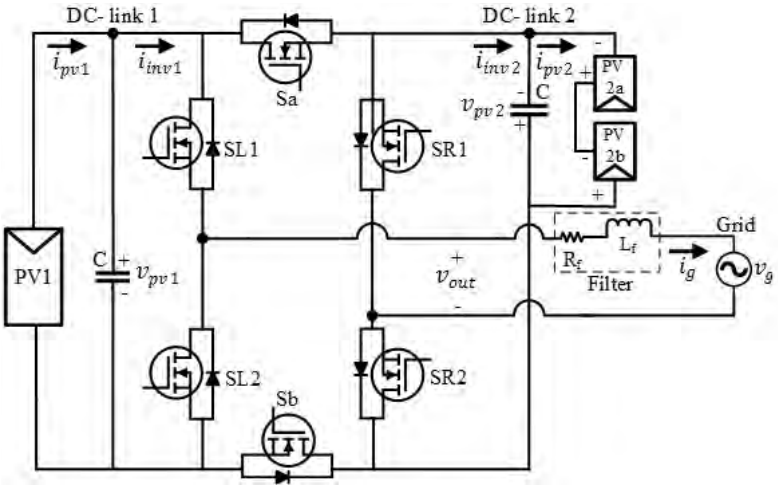

FIGURE 1. Novel H-Bridge based grid connected photovoltaic system.

control technique. The control goals in a GCPS include the extraction of maximum energy from the PV panels and injecting the current with minimum THD into the grid. Considering a MLI based GCPS, several PV panels or array of panels serve as an input voltage source to the inverter through independent DC-links. The maximum power point (MPP) tracking of PV panels is an important control goal due to the fact that MPP of each DC-link may have different operating voltage due to unequal irradiance, temperature and aging of PV panels [14]. THD has to be kept to minimum for the quality of the overall grid. Linear control schemes, like PID, feed-forward etc., with a variety of compensations and modulation methods have been used in CHBMLI based GCPS [10]. Possible drawbacks of classical control scheme includes large transient time and slow response [15]. As an alternative to the classical control schemes and modulation schemes, direct model predictive control (DMPC) is an emerging control scheme used in power electronic converters. In DMPC the switches are controlled directly without the need of demodulator, as in PWM control [16]. Some of the advantages of DMPC are that it can handle plant nonlinearities, multiple inputs, multiple control goals, and any constraints on inputs/states while guaranteeing optimal control. Moreover, it also exhibits fast transient response [17].

In this paper we propose the DMPC of the novel H-Bridge based GCPS. The key idea is to benefit from both the advantages of novel H-Bridge and DMPC to have an overall improved performance of the GCPS. The complete system is compared with existing work of DMPC on GCPS with other topologies.

II. NOVEL H-BRIDGE BASED GCPS

The main circuit of the novel H-Bridge topology based GCPS is shown in Fig 1. It consists of PV panel modules [18] as an input along with the DC-link capacitors, the multilevel inverter, a filter and grid. A simple passive low-pass inductor filter Lf is used at the grid side along with its equivalent series resistance Rf to compensate inductor losses. For safety purposes or to avoid hazard, if required, an isolation can be inserted at the grid side via isolation transformer, which should be able to operate at a low frequency or frequency of the grid [19]. For the simplicity of the design, low design cost, less bulky design, and to avoid transformer losses the transformer-less version of the novel H-bridge based GCPS is chosen [20], [21].

Novel H-Bridge MLI topology comprises of six current bi-directional switches preferably MOSFETs or IGBTs and it is able to generate seven voltage levels if the magnitude of the voltage source v_{pv2} is roughly twice that of v_{pv1}. To achieve this, two solar panels ($PV2a$ and $PV2b$) are connected in series as in [11]. The voltage magnitude of the PV panels doesn't have to be exactly identical to achieve seven-voltage levels at the output of the converter. Following the switching combinations depicted in Table 1, the possible voltage levels are: $0, v_{pv1}, v_{pv2}, (v_{pv1} + v_{pv2}), -v_{pv1}, -v_{pv2}$, and $-(v_{pv} + v_{pv2})$. In the table, 0 and 1 represent the OFF and ON position of the switches.

TABLE 1. Switching sequence for novel H-Bridge MLI.

Index j	Switching sequence S(j)			v_{out}
	$SL1, SL2$	$SR1, SR2$	Sa, Sb	
1	0,1	0,1	1,0	-$(v_{pv1} + v_{pv2})$
2	0,1	1,0	0,1	v_{pv2}
3	0,1	1,0	1,0	-v_{pv1}
4	1,0	0,1	0,1	v_{pv1}
5	1,0	0,1	1,0	-v_{pv2}
6	1,0	1,0	0,1	$(v_{pv1} + v_{pv2})$
7	1,0	1,0	1,0	0

III. MODELING OF THE PROPOSED GCPS

The controlled states in the proposed system are grid current and DC-link voltages. The model can be derived by using basic circuit analysis techniques. If we apply Kirchhoff's

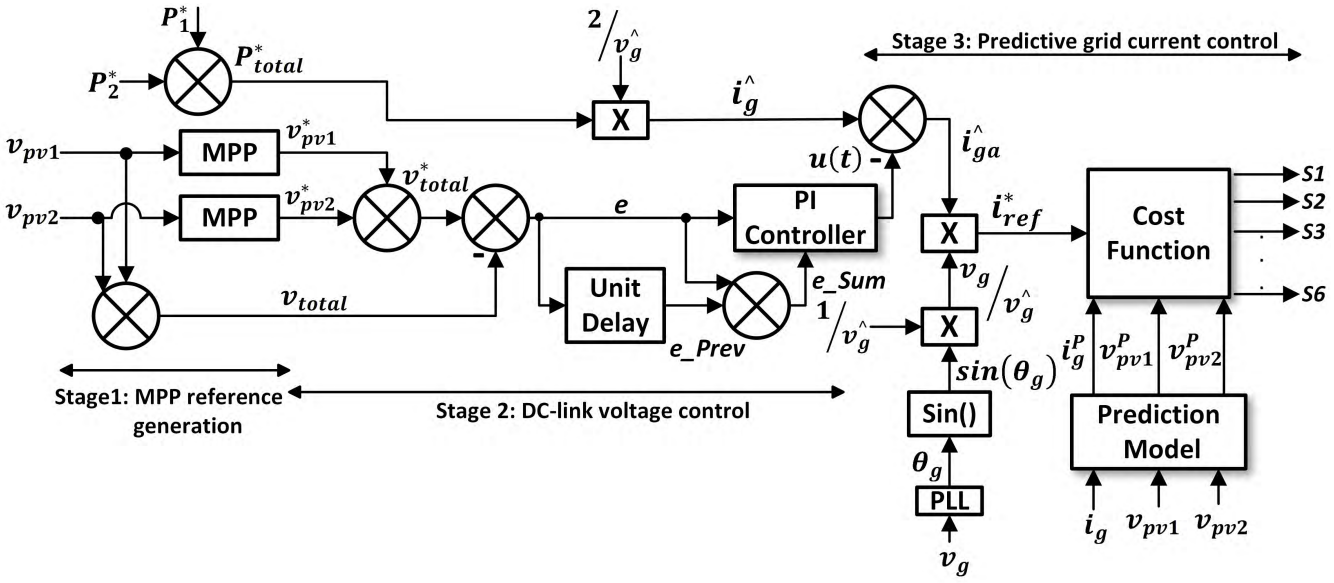

FIGURE 2. The controller block diagram.

Voltage Law (KVL) at the output port of the proposed system in Fig. 1 we get

$$L\, di_g/dt = v_{out} - i_g * R_f - v_g \tag{1}$$

where v_{out} is the output voltage of the MLI, v_g is the grid voltage, and i_g is the grid current. Discretization of the above equation by Euler's forward method yields the prediction equation for the grid current, which is

$$i_g^P = i_g(k+1) = i_g(k)(1 - \frac{R_f * T_s}{L}) + \frac{T_s}{L}(v_{out}(k) - v_g(k)) \tag{2}$$

where $i_g(k)$ and $i_g(k+1)$ are the values of grid current at time instant k and $k+1$; and T_s is the switching time.

The equations for the DC-link voltages (v_{pv1} and v_{pv2}) can be derived by applying Kirchhoff's current law (KCL) at the nodes of DC-link 1 and 2. The equations are given below:

$$C\, dv_{pv1}/dt = i_{pv1}(k) - i_{inv1}(k) \tag{3a}$$
$$C\, dv_{pv2}/dt = i_{pv2}(k) - i_{inv2}(k) \tag{3b}$$

Discretization of the above equations yields

$$v_{pv1}^P = v_{pv1}(k+1) = v_{pv1}(k) + \frac{T_s}{C}(i_{pv1}(k) - i_{inv1}(k)) \tag{4a}$$
$$v_{pv2}^P = v_{pv2}(k+1) = v_{pv2}(k) + \frac{T_s}{C}(i_{pv2}(k) - i_{inv2}(k)) \tag{4b}$$

where $v_{pv1}(k)$ is the value of DC-link 1 voltage, $v_{pv2}(k)$ is the value of DC-link 2 voltage, $i_{pv1}(k)$ is the output current of $PV1$, $i_{pv2}(k)$ is the output current of series connected modules ($PV2a$ and $PV2b$), $i_{inv1}(k)$ and $i_{inv2}(k)$ are the input currents of MLI, and C is the value of DC-link capacitors. The output current of MLI could be either $i_g(k)$, 0, or $-i_g(k)$. By KCL, the total input current of the MLI can also have either of these three values depending upon the switching scheme.

IV. PROPOSED CONTROL SCHEME

The proposed control scheme is depicted in Fig. 2. It consists of three stages: 1) MPP reference generation of the PV panels, 2) DC-link voltage control, and 3) model predictive control of injected grid current. The starting two stages, being standard in conventional PV systems, are not a component of proposed DMPC scheme [9], [22]. The foremost contribution of this research work is the DMPC for the grid current control. The coming discussion will briefly describe the first two stages before the explanation of the third stage.

The first stage involves the calculation of reference values for the DC-link voltages (v_{pv1}^* & v_{pv2}^*) and power (P_1^* & P_2^*). This stage ensures that these reference values are for the MPP despite of changes in atmospheric conditions [23]. Generally, Perturb and Observe (P&O) algorithm is used for the MPP reference generation at this stage [24]. The reference and the actual voltage values are combined together to compute the DC-link voltage error (e) to be used afterwards in stage 2 i.e. the DC-link voltage control. Also, the individual reference power values for all the PV panels are added to compute the nominal power of the system which is used later in reference grid current calculation.

The second stage of the proposed control scheme generates the reference grid current, which is required in stage 3. In case of deviation in combined DC-link voltages from their combined MPP reference value i.e. e, the reference grid current is adjusted accordingly. This stage uses a linear PI controller to help attain DC-link voltages at their reference

values by adjusting the reference peak value of grid current $\hat{i}_g$. The reference peak value of grid current depends on the nominal power of the system P^*_{total} [9] in stage 1. It is calculated as $\hat{i}_g = (P^*_{total}/\hat{v}_g)*2$. The adjusted peak value of grid current, which is denoted as $\hat{i_{ga}}$ in Fig. 2, is computed by the addition of peak current $\hat{i}_g$ with the output of the PI controller. At the end, the instantaneous reference of the grid current i^*_{ref} is quantified based on the adjusted peak reference $\hat{i_{ga}}$ and phase locked loop (PLL).

The third stage ensures the reference tracking of grid current by selecting an optimal switching combination for MLI. DMPC makes use of the discrete model of the converter to calculate the optimal switching state among the finite number of switching positions. DMPC can handle multiple control goals, it is easy to implement, and it restricts the requirement of a modulator by the direct manipulation of semiconductor switches. Moreover, it attains a fast dynamic response and gives a fast and robust current tracking capability.

The cost function for the direct model predictive control is given as

$$g = \lambda_i |i^*_g - i_g(k+1)| + \lambda_v [\sum_{k=1}^{n} |v^*_{pvk} - v_{pvk}(k+1)|] \quad (5)$$

where i^*_g and v^*_{pvk} are the reference values for the grid current and DC-link voltages; and n is the total number of input DC sources or DC-links, which are two in the present case. The cost function includes two control objectives/goals: 1) to track the reference of grid current, and 2) to track the individual reference of DC-link voltages. The control goals are selected to ensure the reference tracking of both the grid current and the individual DC-link voltages. It is to be noted that the third stage ensures the individual DC-link voltage control for each PV panel while second stage involves in the combined DC-link voltage control for the PV panels. The references for the DC-link voltages and the grid current are generated in stage 1 and stage 2 of the proposed control scheme respectively. To set the relative priority of control goals the values of weighing factors λ_i and λ_v are adjusted. The flowchart of the DMPC algorithm is shown in Fig. 3. The proposed control algorithm starts with the measurement of controlled variables i.e. grid current and DC-link voltages and their reference values. The initial best known cost is kept to be a very large number. Among the seven possible switching combinations, which are listed in Table 1, the algorithm has to find the one that gives the lowest cost.

For each switching combination the output voltage of converter is found by using Table 1. The discrete-time model along with the value of the output voltage is used to calculated the values of grid current and DC Link voltages at time instant $k+1$. These values can be used to compute the cost in eq. (5). If the cost is less than the best known/optimal cost so far, then the optimal cost and optimal switching sequence are updated. At the end, the optimal switching sequence is applied to the converter.

TABLE 2. System parameters.

Variable	Definition	Value
P_{total}	Nominal input power	624.1 W
v^*_{pv1}	Reference DC-link 1 voltage	28.5 V
v^*_{pv2}	Reference DC-link 2 voltage	57 V
f	Frequency of grid	50 Hz
f_s	Switching/Sampling frequency	20 kHz
L_f	Filtering inductor	3 mH
R_f	ESR	0.2 Ω
C	DC-link capacitor	15 mF
$\hat{v}_g$	Peak grid voltage	70 V

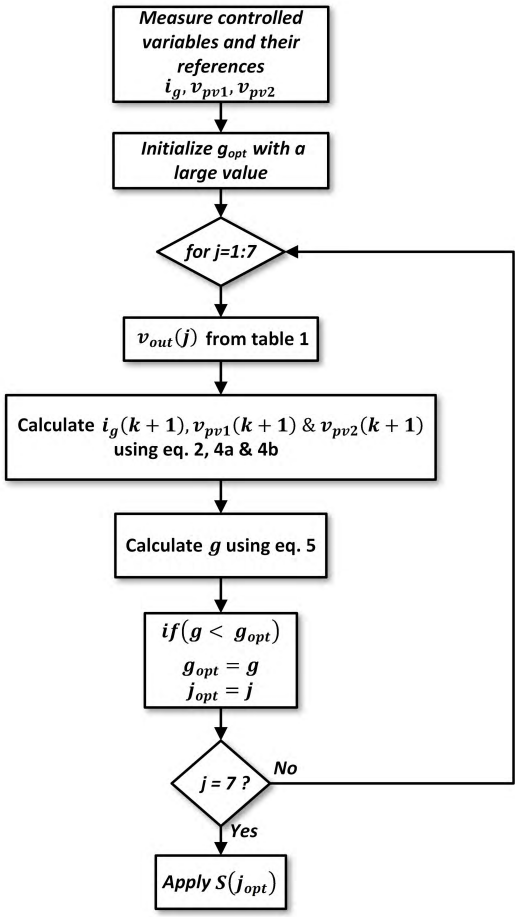

FIGURE 3. Flow diagram of the proposed control scheme.

V. SIMULATION RESULTS

The complete system is simulated in Simulink, MATLAB using the proposed control scheme. The PV panel modules "Sharp ND-208U2" are used as input sources. The rated maximum power of PV panels is 208.05 Watts at 28.5V and 7.3A. There are three PV modules, which are $PV1$, $PV2a$ & $PV2b$. The value of DC-link capacitors is $15mF$. The inductive ac filter has inductance and resistance of $3mH$ and 0.2Ω. The other design and simulation parameters are given in Table 2.

To observe the dynamic behavior of the proposed control scheme, step changes in the input parameters, i.e. solar

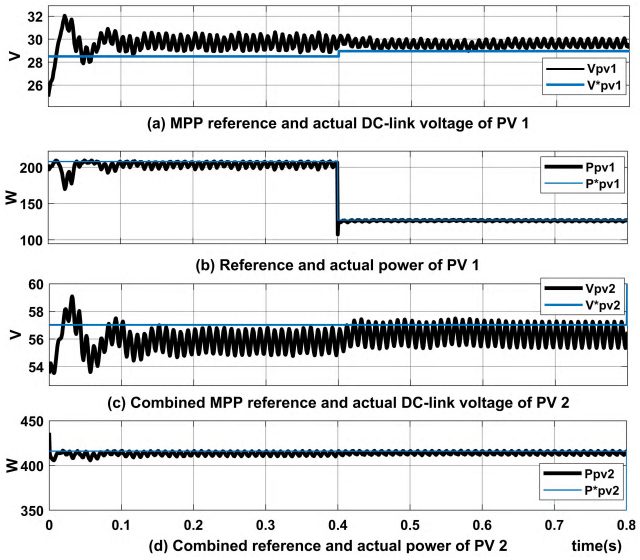

FIGURE 4. Step change in solar irradiance of *PV 1*.

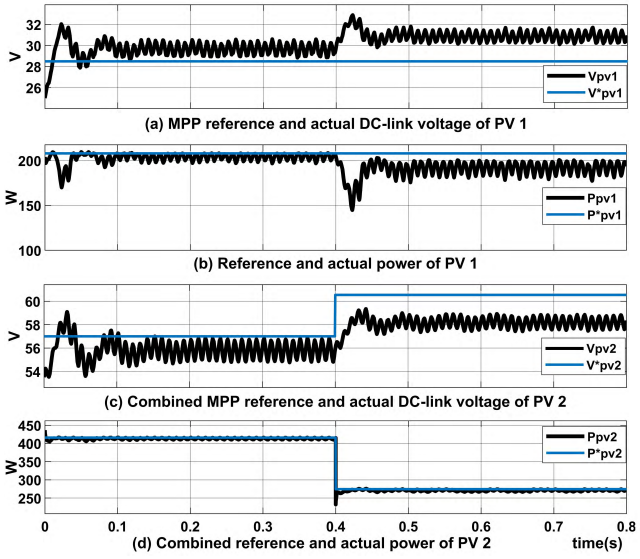

FIGURE 5. Step change in solar irradiance of *PV 2a*.

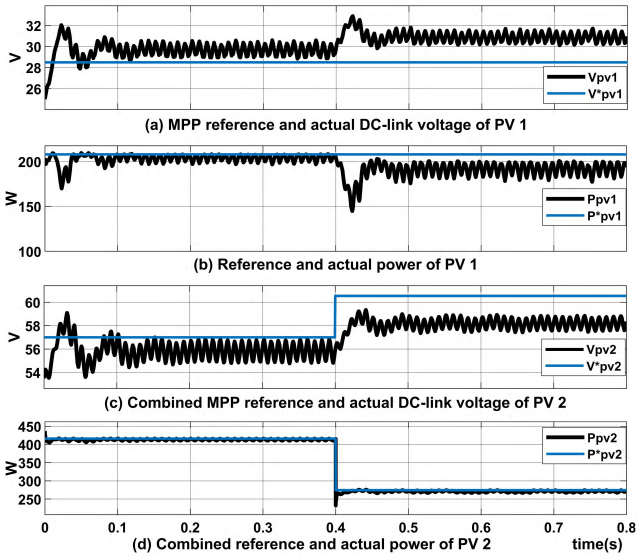

FIGURE 6. Step change in solar irradiance of *PV 2b*.

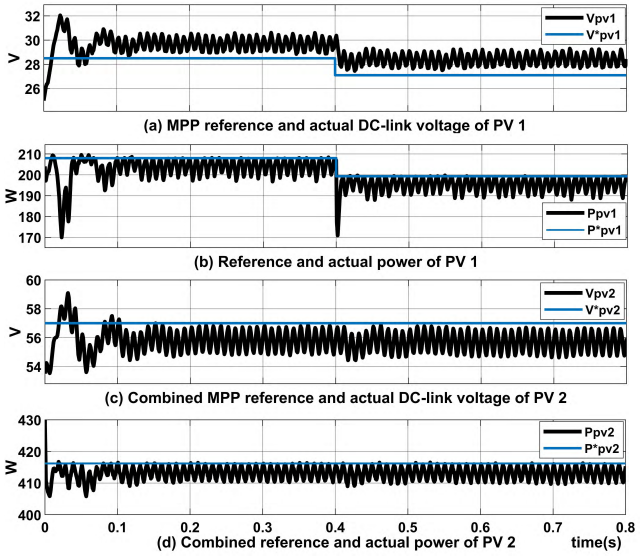

FIGURE 7. Step change in temperature of *PV 1*.

irradiance and temperature, of the PV modules are simulated and the results are collected. Coming subsections discusses the simulation results of the proposed system. In each subsection, a step change is applied in one of the input parameter of a different PV module. The starting input atmospheric conditions of the PV modules in all the subsections are $1000W/m^2$ irradiance and $25°C$ temperature. The respective MPP reference voltage and power values of the PV modules at the starting input conditions are 28.5V and 208.05W respectively.

A. STEP CHANGE IN SOLAR IRRADIANCE OF PV 1

In this subsection, at $t = 0.4$s, the solar irradiance of the module $PV1$ is changed from 1000 to $600W/m^2$. Doing so, as per MPP, the reference voltage of $PV1$ increases to 28.96V and its reference power reduces to 127.3W. The actual voltage and power of $PV1$ follow their references respectively as depicted in Fig. 4.

B. STEP CHANGE IN SOLAR IRRADIANCE OF PV 2A & PV 2B

In this subsection, the solar irradiance of the module $PV2a$ is changed from 1000 to $600W/m^2$ at $t = 0.4$s. As a result, the reference voltage of series connected PV modules increases from 57V to 60.54V and their reference power changes from 416.1W to 274.4W. The combined actual voltage and power of $PV2$ follow their references as shown in Fig. 5. In the figure, we also see that a small effect of change in input parameters in $PV2a$ is visible in the voltage

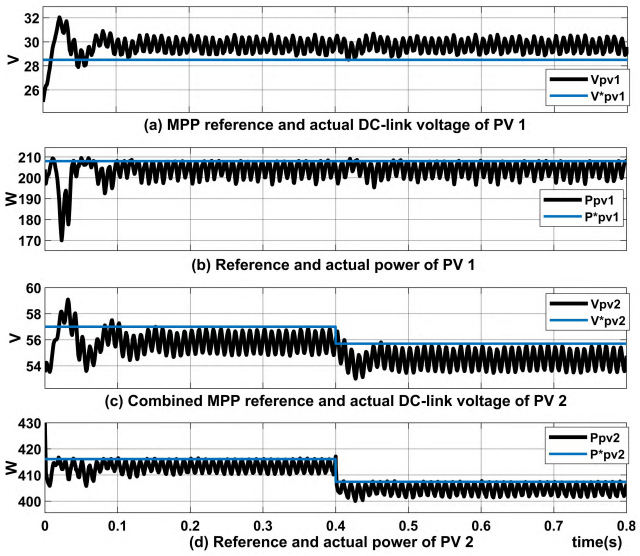

FIGURE 8. Step change in temperature of *PV 2a*.

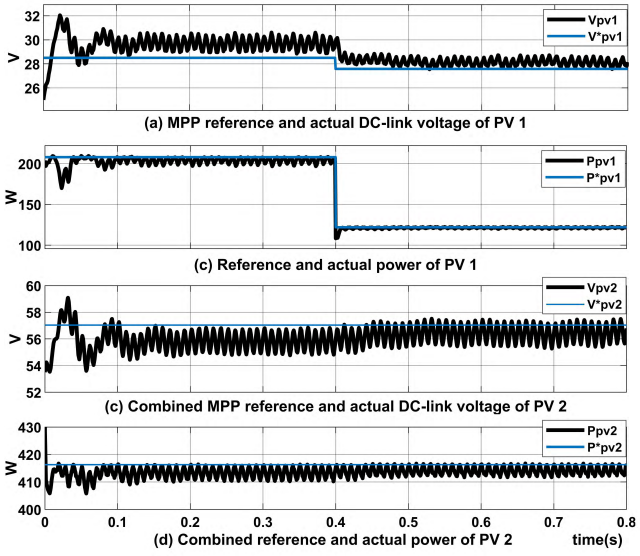

FIGURE 9. Step change in solar irradiance and temperature of *PV 1*.

and power response of $PV1$. It is due to the usage of combined reference voltage for the DC-link voltage control. Similarly, same results are achieved when the step change in solar irradiance is introduced in $PV2b$ at $t = 0.4$s as shown in Fig. 6.

C. STEP CHANGE IN TEMPERATURE OF PV 1

In this subsection, after keeping the starting input conditions of the PV modules at $1000W/m^2$ irradiance and $25°C$ temperature, the temperature of $PV1$ is changed to $35°C$ at $t = 0.4$s. The effect of increase in temperature causes reduction in the reference voltage from 28.5V to 27.18V and change in reference power from 208.05W to 199.3W. Again, the references of $PV1$ are followed by the actual voltage and power values as presented in Fig. 7.

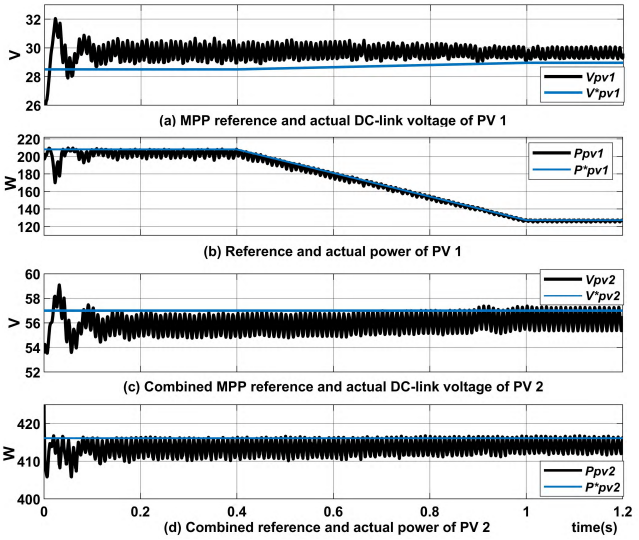

FIGURE 10. Change in solar irradiance of *PV 1* as a negative ramp function.

TABLE 3. Comparison of systems in terms of current and voltage THD and number of switches.

Feature, GCPS	DMPC and basic CHB based GCPS [9]	DMPC and topology in [11] based GCPS [12]	Proposed DMPC and novel H-Bridge based GCPS
Grid current harmonics (%)	1.5 - 2	2.7 - 3.1	2.5 - 2.7
Output voltage harmonics (%)	28 - 30	29 - 36	24 - 32
Number of switches @7-levels	12	9	6

D. STEP CHANGE IN TEMPERATURE OF PV 2A

At $t = 0.4$s, the temperature of $PV2a$ is changed from $25°C$ to $35°C$ in this subsection. In these conditions, the combined reference voltage and power values changes to 407.4W and 55.7V respectively. The actual values follow them as shown in Fig. 8.

E. STEP CHANGE IN SOLAR IRRADIANCE AND TEMPERATURE OF PV 1

In this subsection, both solar irradiance and temperature of $PV1$ are varied from $1000W/m^2$ and $25°C$ to $600W/m^2$ and $35°C$ at $t = 0.4$s. As a result, the reference voltage and power values reforms in to 122W and 27.58V. The references are followed by the actual values once again as shown in Fig. 9.

F. CHANGE IN SOLAR IRRADIANCE OF PV 1 AS NEGATIVE RAMP FUNCTION

In this subsection, the solar irradiance of $PV1$ is changed from $1000W/m^2$ to $600W/m^2$ as a negative ramp function at $t = 0.4$s. In the results shown in Fig. 10, we see that the

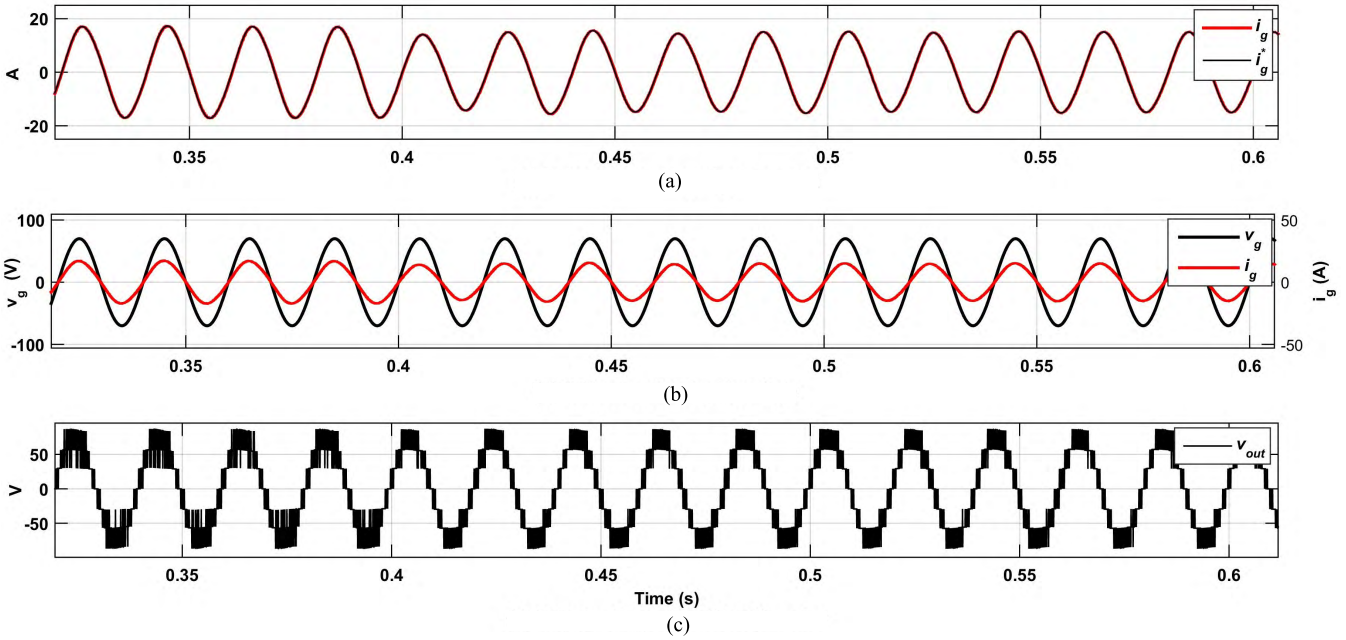

FIGURE 11. Grid current, grid voltage, and output voltage of multilevel inverter.

TABLE 4. Comparison of systems in terms of efficiency.

GCPS	DMPC and basic CHB based GCPS [9]			DMPC and topology in [11] based GCPS [12]			Proposed DMPC and novel H-Bridge based GCPS		
Time, Feature	MPPT efficiency η_{mppt} %	Inverter efficiency η_{inv} %	Overall efficiency η_{oa} %	MPPT efficiency η_{mppt} %	Inverter efficiency η_{inv} %	Overall efficiency η_{oa} %	MPPT efficiency η_{mppt} %	Inverter efficiency η_{inv} %	Overall efficiency η_{oa} %
0<t<0.4s	99.67	86.01	**85.73**	98.23	88.09	**86.53**	99.03	95.43	**93.75**
0.4<t<0.8s	99.55	86.87	**86.49**	99.74	89.48	**89.25**	99.74	95.01	**94.77**
0.8<t<1.2s	99.70	86.67	**86.41**	99.60	89.55	**89.20**	99.60	95.14	**94.77**
1.2<t<1.6s	99.57	90.66	**90.28**	95.06	92.17	**87.62**	97.84	96.33	**94.26**
1.6<t≤2s	99.72	90.41	**90.16**	95.90	92.59	**88.79**	98.08	96.10	**94.26**

actual voltage and power values of $PV1$ accompanies their reference values.

G. EFFECT OF STEP CHANGES ON GRID CURRENT

The performance of the other control goal which is the reference grid current tracking is shown in Fig. 11(a). At $t = 0.4$s the reference grid current changes due to the change in reference power and the actual grid current follows its reference. The combined waveform of grid voltage and current is shown in Fig. 11(b) which have no phase difference between them despite of changes in atmospheric conditions. The seven-level output voltage waveform of novel H-Bridge MLI is shown in Fig. 11(c).

Novel H-Bridge MLI topology based GCPS controlled by the proposed DMPC scheme is compared with other MLI topologies based GCPS. The results are given in Table 3, 4 and Fig. 12. The other MLI topologies which are the basic CHB and the topology in [11] based GCPS's [9], [12] are also controlled with a DMPC scheme. The comparison in Table 3 enlists the harmonic content of grid current and output voltage of MLI, and the number of semi-conductor switches used. The graphical comparison in Fig. 12 shows the total reference MPP power ($Pmpp$) as per stage 1 of the proposed DMPC scheme, the total power extracted from PV panels ($Pext.$), and the output power ($Pout$) in different atmospheric conditions. In Fig. 12, the starting simulation conditions for all the PV panels in the GCPS are $1000W/m^2$ irradiance and $25°C$ temperature. At $t = 0.4$s, the solar irradiance of $PV1$ is changed from $1000W/m^2$ to $600W/m^2$ and its temperature is changed from $25°C$ to $35°C$ at $t = 0.8$s. The solar irradiance and temperature of both PV modules in $PV2$ is changed at $t = 1.2$s and $t = 1.6$s, respectively. At each of the simulation condition, the MPP reference power is adjusted and the total power extracted from PV panels gets regulated accordingly. The output power is calculated as $Pout = Vgrid * ig$. The comparison in Table 4 enlists the efficiency of MPPT η_{mppt}, the inverter η_{inv}, and the overall system η_{oa}. The MPPT efficiency, inverter efficiency, and overall efficiency are defined as $\eta_{mppt} = Pext./Pmpp * 100$, $\eta_{inv} = Pout./Pext. * 100$, and $\eta_{oa} = Pout./Pmpp * 100$, respectively.

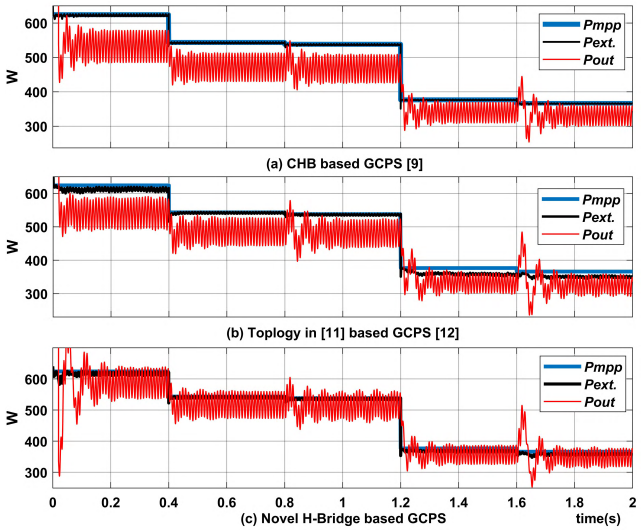

FIGURE 12. Comparison between GCPS in terms of total reference MPP power, extracted power from PV panels and output power.

The system in [9] offers the best current harmonics and power extraction i.e. the MPPT efficiency. The reason is that in basic CHBMLI topology each PV module is connected independently, i.e. there is no series connection, which allows better MPP tracking [3], [10]. However, the increased number of semiconductor switches in the topology reduces the efficiency of power transfer to the grid. In terms of the voltage harmonics, number of switches, the inverter efficiency, and the overall efficiency, the proposed systems is better than [9]. Moreover, the proposed system is better than [12] in all aspects of the comparison.

VI. CONCLUSION

In this paper, a direct model predictive control scheme for grid current is presented for the novel H-Bridge MLI based GCPS. The proposed system offers a high efficiency as compared to the reported systems in literature. Simulation results also show that the proposed system has a comparable/better performance in terms of THD and power extraction.

REFERENCES

[1] S. B. Kjaer, J. K. Pedersen, and F. Blaabjerg, "A review of single-phase grid-connected inverters for photovoltaic modules," *IEEE Trans. Ind. Appl.* vol. 41, no. 5, pp. 1292–1306, Sep./Oct. 2005.

[2] V. N. Lal and S. N. Singh, "Control and performance analysis of a single-stage utility-scale grid-connected PV system," *IEEE Syst. J.* vol. 11, no. 3, pp. 1601–1611, Sep. 2017.

[3] S. Kouro, J. I. Leon, D. Vinnikov, and L. G. Franquelo, "Grid-connected photovoltaic systems: An overview of recent research and emerging PV converter technology," *IEEE Ind. Electron. Mag.*, vol. 9, no. 1, pp. 47–61, Mar. 2015.

[4] E. Babaei, S. Alilu, and S. Laali, "A new general topology for cascaded multilevel inverters with reduced number of components based on developed H-bridge," *IEEE Trans. Ind. Electron.*, vol. 61, no. 8, pp. 3932–3939, Aug. 2014.

[5] S.-A. Amamra, K. Meghriche, A. Cherifi, and B. Francois, "Multilevel inverter topology for renewable energy grid integration," *IEEE Trans. Ind. Electron.* vol. 64, no. 11, pp. 8855–8866, Nov. 2017.

[6] J. Rodriguez, J.-S. Lai, and F. Z. Peng, "Multilevel inverters: A survey of topologies, controls, and applications," *IEEE Trans. Ind. Electron.*, vol. 49, no. 4, pp. 724–738, Aug. 2002.

[7] L. G. Franquelo, J. Rodriguez, J. I. Leon, S. Kouro, R. Portillo, and M. A. M. Prats, "The age of multilevel converters arrives," *IEEE Ind. Electron. Mag.*, vol. 2, no. 2, pp. 28–39, Jun. 2008.

[8] T. Muhammad, A. U. Khan, M. Luqman, M. B. Satti, M. Aaqib, and M. F. Khan, "Generation of isolated DC voltage sources for multilevel inverters," in *Proc. Power Gener. Syst. Renew. Energy Technol. (PGSRET)*, Jun. 2015, pp. 1–6.

[9] P. Cortes, S. Kouro, F. Barrios, and J. Rodriguez, "Predictive control of a single-phase cascaded h-bridge photovoltaic energy conversion system," in *Proc. 7th Int. Power Electron. Motion Control Conf.*, vol. 2, Jun. 2012, pp. 1423–1428.

[10] E. Villanueva, P. Correa, J. Rodriguez, and M. Pacas, "Control of a single-phase cascaded H-bridge multilevel inverter for grid-connected photovoltaic systems," *IEEE Trans. Ind. Electron.*, vol. 56, no. 11, pp. 4399–4406, Nov. 2009.

[11] M. Mousa, M. E. Ahmed, and M. Orabi, "New converter circuitry for PV applications using multilevel converters," in *Proc. 31st Int. Telecommun. Energy Conf.*, Oct. 2009, pp. 1–6.

[12] M. Mosa, H. Abu-Rub, M. E. Ahmed, A. Kouzou, and J. Rodríguez, "Control of single phase grid connected multilevel inverter using model predictive control," in *Proc. 4th Int. Conf. Power Eng. Energy Elect. Drives*, May 2013, pp. 624–628.

[13] E. Babaei, S. Laali, and S. Alilu, "Cascaded multilevel inverter with series connection of novel H-bridge basic units," *IEEE Trans. Ind. Electron.*, vol. 61, no. 12, pp. 6664–6671, Dec. 2014.

[14] R. P. Aguilera *et al.*, "Predictive control algorithm to achieve power balance of cascaded H-bridge converters," in *Proc. IEEE Int. Symp. Predictive Control Elect. Drives Power Electron. (PRECEDE)*, Oct. 2015, pp. 49–54.

[15] S. Vazquez, J. Rodriguez, M. Rivera, L. G. Franquelo, and M. Norambuena, "Model predictive control for power converters and drives: Advances and trends," *IEEE Trans. Ind. Electron.*, vol. 64, no. 2, pp. 935–947, Feb. 2017.

[16] A. Ayad, P. Karamanakos, and R. Kennel, "Direct model predictive current control strategy of quasi-Z-source inverters," *IEEE Trans. Power Electron.*, vol. 32, no. 7, pp. 5786–5801, Jul. 2016.

[17] J. Rodriguez *et al.*, "State of the art of finite control set model predictive control in power electronics," *IEEE Trans. Ind. Informat.*, vol. 9, no. 2, pp. 1003–1016, May 2013.

[18] M. A. G. de Brito, L. P. Sampaio, L. G. Junior, and C. A. Canesin, "Research on photovoltaics: Review, trends and perspectives," in *Proc. Brazilian Power Electron. Conf.*, Sep. 2011, pp. 531–537.

[19] S. Rivera, S. Kouro, B. Wu, J. I. Leon, J. Rodríguez, and L. G. Franquelo, "Cascaded H-bridge multilevel converter multistring topology for large scale photovoltaic systems," in *Proc. IEEE Int. Symp. Ind. Electron.*, Jun. 2011, pp. 1837–1844.

[20] H. Jedtberg, A. Pigazo, M. Liserre, and G. Buticchi, "Analysis of the robustness of transformerless PV inverter topologies to the choice of power devices," *IEEE Trans. Power Electron.*, vol. 32, no. 7, pp. 5248–5257, Jul. 2017.

[21] Y. P. Siwakoti and F. Blaabjerg, "H-bridge transformerless inverter with common ground for single-phase solar-photovoltaic system," in *Proc. IEEE Appl. Power Electron. Conf. Expo. (APEC)*, Mar. 2017, pp. 2610–2614.

[22] L. Huang, D. Qiu, F. Xie, Y. Chen, and B. Zhang, "Modeling and stability analysis of a single-phase two-stage grid-connected photovoltaic system," *Energies*, vol. 10, no. 12, p. 2176, 2017.

[23] H. P. Desai and H. K. Patel, "Maximum power point algorithm in PV generation: An overview," in *Proc. 7th Int. Conf. Power Electron. Drive Syst.*, Nov. 2007, pp. 624–630.

[24] D. P. Hohm and M. E. Ropp, "Comparative study of maximum power point tracking algorithms using an experimental, programmable, maximum power point tracking test bed," in *Proc. Conf. Rec. 28th IEEE Photovoltaic Spec. Conf.*, Sep. 2000, pp. 1699–1702.

MUHAMMAD BILAL SATTI was born in Pakistan in 1993. He received the B.E. degree in electronics engineering from International Islamic University, Islamabad, Pakistan, in 2015, and the master's degree in electrical engineering with focus on power electronics and control systems from the National University of Sciences and Technology, Islamabad, in 2018. His current research interests include model predictive control, control of power electronic converters, and multilevel inverters.

AMMAR HASAN was born in Pakistan, in 1982. He received the B.E. degree in electrical engineering from the National University of Sciences and Technology, Islamabad, Pakistan, in 2004, and the master's and Ph.D. degrees in control systems from the Imperial College London, London, U.K., in 2008 and 2012, respectively.

Since 2012, he has been with the School of Electrical Engineering and Computer Science, National University of Sciences and Technology, where he is currently an Associate Professor. His current research interests include model predictive control, control of power electronic converters, and optimization techniques for control systems.